



# In vitro biomolecular interaction studies and cytotoxic activities of copper(II) and zinc(II) complexes bearing ONS donor thiosemicarbazones

Nimya Ann Mathews<sup>1</sup> | M.R. Prathapachandra Kurup<sup>1,2</sup>

<sup>1</sup>Department of Applied Chemistry, Cochin University of Science and Technology, Kochi, India

<sup>2</sup>Department of Chemistry, School of Physical Sciences, Central University of Kerala, Periyar, Kasaragod, India

## Correspondence

M.R. Prathapachandra Kurup, Department of Applied Chemistry, Cochin University of Science and Technology, Kochi 682 022, Kerala, India. Email: mrp@cukerala.ac.in

## Funding information

University Grants Commission, Grant/Award Number: CSIR-UGC NET JUNE 2017; Sophisticated Analytical Instrumentation Facility, Cochin University of Science and Technology, Kochi, India; Department of Chemistry, Gandhigram Rural Institute (Deemed to be University); University Grants Commission, New Delhi, India

Among all the bio-metals, zinc and copper derivatives of ONS donor thiosemicarbazone have aroused great interest because of their potential biological applications. Multisubstituted thiosemicarbazone ligand H<sub>2</sub>dspt (3,5-dichlorosalicylaldehyde-N<sup>4</sup>-phenylthiosemicarbazone) derived new ternary complexes like [Zn(dspt)(phen)]·DMF (**1**) and [Cu(dspt)(phen)]·DMF (**2**), and another thiosemicarbazone, H<sub>2</sub>dsct (3,5-dichlorosalicylaldehyde-N<sup>4</sup>-cyclohexylthiosemicarbazone), derived [Cu(dsct)(bipy)]·DMF (**3**). These complexes have been characterized by elemental analysis (CHNS), Fourier transform infrared (FT-IR), ultraviolet-visible (UV-Vis) and proton nuclear magnetic resonance (<sup>1</sup>H-NMR) spectra. The structures of the complexes were obtained by single-crystal X-ray diffraction analysis. Compounds **1** and **2** got crystallized in the monoclinic *P*<sub>2</sub><sub>1</sub>/*c* space group. The complexes showed interesting supramolecular interaction, which in turn stabilizes the complexes. The ground state electronic configurations of the complexes were studied using the B3LYP/LANL2DZ basis set, and ESP plots of complexes were investigated. The interaction of the complexes with calf thymus DNA (CT-DNA) was studied using absorption and fluorescence spectroscopic methods. A UV study of the interaction of the complexes with calf thymus DNA (CT-DNA) has shown that the complexes can effectively bind to CT-DNA, and [Cu(dspt)(phen)]·DMF (**2**) exhibited the highest binding constant to CT-DNA ( $K_b = 3.7 \times 10^4$ ). Fluorescence spectral studies also indicated that Complex **2** binds relatively stronger with CT DNA through intercalative mode, exhibiting higher binding constant ( $K_q = 4.7 \times 10^5$ ). The DNA cleavage result showed that the complexes are capable of cleaving the DNA without the help of any external agent. Molecular docking studies were carried out to understand the binding of complexes with the molecular target DNA. Complex **2** exhibited the highest cytotoxicity against human breast cancer cell line MD-MBA-231 ( $IC_{50} = 23.93 \mu\text{g/mL}$ ) as compared to Complex **1** ( $IC_{50} = 44.40 \mu\text{g/mL}$ ).

## KEYWORDS

cytotoxicity evaluation, DNA binding, molecular docking, thiosemicarbazone complexes, X-ray

## 1 | INTRODUCTION

Coordination compounds have tremendous applications in various fields of science. The discovery of cisplatin, that is, cis-[dichlorodiammine] platinum(II), made possible the usage of metals in the medical field.<sup>[1]</sup> Thiosemicarbazones usually act as chelating agents with transition and nontransition metal ions connected through sulfur and nitrogen atoms and have immense pharmaceutical applications. Studies on copper and iron complexes show an active hindrance for the DNA synthesis than in the case of metal-free thiosemicarbazone.<sup>[2]</sup> Copper complexes of thiosemicarbazones exhibit interesting structures.<sup>[3]</sup> Antitumor activities of some transition metal complexes of thiosemicarbazone derived from 3-acetyllumbiferone were also explored.<sup>[4]</sup> Ligand systems with ONS donor atoms are found to have sufficient carcinostatic potency. Among the metals, copper and zinc are the essential trace metals required for organisms to perform several important biological processes. Their chelates have been studied very effectively as less toxic alternatives and are very selective in anticancer treatments.<sup>[5]</sup>

The interactions of metal complexes with DNA are important for the development of effective chemotherapeutic agents. Transition metal centers, particularly copper complexes, can bind to DNA through various covalent and noncovalent interactions.<sup>[5]</sup> The reported covalent interaction is *via* the coordination of copper with the N-7 of the purine base and the phosphate group of a polynucleotide chain.<sup>[5]</sup> Barone et al. gave an excellent review on the DNA-binding ability of Cu and Zn complexes.<sup>[6]</sup> It is reported that the complexes that have bulky ligands interact with DNA in groove binding mode whereas complexes that have planar aromatic groups interact with DNA in the intercalative mode of binding. Thus, the ligand moiety plays a vital role in studying DNA interactions with complexes.<sup>[7]</sup>

Cancer is believed to be a family of diseases that involves abnormal cell growth and can spread to various parts of the body. The drugs involved in its treatment are toxic and can affect the normal functioning of DNA in the cells. Developing anticancer drugs with high efficacy and low toxicity are the most important challenges these days. On the basis of the effect of zinc and copper on cancer progression, chelators that bind metal have been developed as anticancer agents. There are many reports in which metal complexes bind with the bipyridyl ligands. Bipyridyl-containing metal complexes are excellent antitumor agents that enhances the planarity of the molecule and thereby strengthen the binding ability of the complex.<sup>[8]</sup> Thus, the development of less toxic and cost-effective anticancer drugs has emerged as an essential area in pharmaceutical research.

All the above facts motivated us to develop zinc and copper-based complexes of thiosemicarbazone derivatives with 1,10-phenanthroline and 2,2'-bipyridine acting as co-ligands and we evaluated their DNA binding, cleavage and cytotoxicity. Even though many copper and zinc complexes are known already, our focus is to develop better biologically active complexes. The synthesis and characterization of Complex **3** is already reported from our group, and our current focus is more toward its DNA binding and cleavage property.

## 2 | EXPERIMENTAL SECTION

### 2.1 | Materials

N<sup>4</sup>-phenyl thiosemicarbazone (Alfa Aesar), 3,5-dichlorosalicylaldehyde, cyclohexylisothiocyanate (Alfa Aesar), hydrazine hydrate (Sigma Aldrich), zinc acetate, and copper acetate were of analytical grade and purchased from commercial sources. The Spectrochem solvents methanol, acetonitrile, and dimethylformamide (DMF) were used without further purification.

### 2.2 | Synthesis of 3,5-dichlorosalicylaldehyde-N<sup>4</sup>-phenylthiosemicarbazone (H<sub>2</sub>dspt)

H<sub>2</sub>dspt is prepared as per an already reported procedure.<sup>[9]</sup>

3,5-Dichlorosalicylaldehyde (0.191 g, 1 mmol) and N<sup>4</sup>-phenylthiosemicarbazone (0.167 g, 1 mmol) in 20 mL acetonitrile are stirred and heated for 2 h after adding a drop of glacial acetic acid. The resulting solution was kept aside and cooled. After some time, a yellow-colored precipitate was formed, filtered, and washed with methanol and dried (Scheme 1).

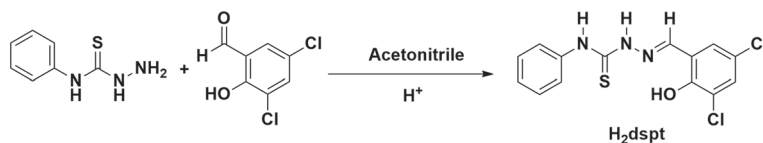
Yield: 0.227 g, 67%. Anal. Calc. for C<sub>14</sub>H<sub>11</sub>N<sub>3</sub>Cl<sub>2</sub>OS (340.23 g mol<sup>-1</sup>): C, 49.42; H, 3.26; N, 12.35; S, 9.42. Found: C, 49.48; H, 3.30; N, 12.39; S, 9.48.

### 2.3 | Synthesis of metal complexes

#### 2.3.1 | [Zn(dspt)(phen)]·DMF (1)

Complex **1** was prepared by refluxing a 20 mL 1:1 mixture of DMF and methanol solution of 3,5-dichlorosalicylaldehyde-N<sup>4</sup>-phenyl thiosemicarbazone (1 mmol, 0.340 g) and zinc acetate (1 mmol, 0.219 g) for 4 h. To this solution, hydrated 1,10-phenanthroline (1 mmol, 0.198 g) in 5 mL methanol was added. The

**SCHEME 1** Synthesis of the proligand ( $H_2dspt$ )



resulting solution was allowed to stand at room temperature and after slow evaporation, yellow-colored block-shaped crystals were separated, filtered and washed with methanol and dried in air (Scheme 2).

Yield: 0.558 g, 85%. Molar conductance ( $10^{-3}$  M DMF):  $10 \Omega^{-1}cm^2mol^{-1}$ . Anal. Calc. for  $C_{29}H_{24}Cl_2N_6O_2SZn$  ( $656.87 g mol^{-1}$ ): C, 53.02; H, 3.68; N, 12.79; S, 4.88. Found: C, 53.08; H, 3.60; N, 12.71; S, 4.82.

### 2.3.2 | [Cu(dspt)(phen)]·DMF (2)

Complex **2** was prepared similar to Complex **1** by refluxing 20 mL 1:1 mixture of DMF and methanol solution of  $H_2dspt$  (1 mmol, 0.340 g), copper acetate (1 mmol, 0.199 g) and hydrated 1,10-phen (1 mmol, 0.198 g) for 4 h. A green precipitate formed was filtered and recrystallized in 5 mL DMF. Dark green-colored block-shaped crystals were obtained and dried in air (Scheme 2).

Yield: 0.504 g, 77%. Molar conductance ( $10^{-3}$  M DMF):  $15 \Omega^{-1}cm^2mol^{-1}$ . Anal. Calc. for  $C_{29}H_{24}N_6Cl_2CuO_2S$

( $655.04 g mol^{-1}$ ): C, 53.17; H, 3.69; N, 12.83; S, 4.89. Found: C, 53.11; H, 3.60; N, 12.88; S, 4.80.

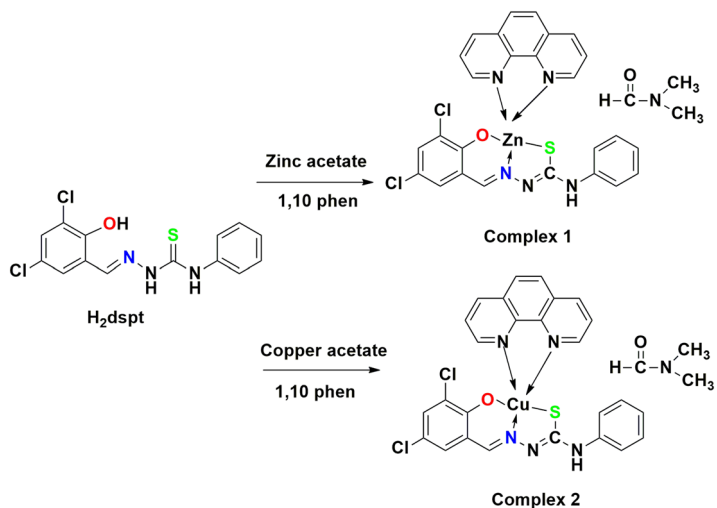
### 2.3.3 | [Cu(dsct)(bipy)]·DMF (3)

[Cu(dsct)(bipy)]·DMF is synthesized as per our previous report<sup>[10]</sup> (Scheme 3).

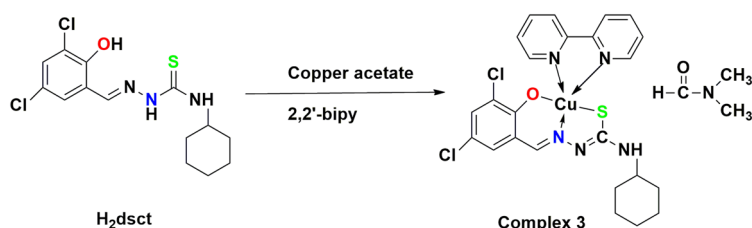
The thiosemicarbazone,  $H_2dsct$  (1 mmol, 0.346 g) was dissolved in 1:1 methanol and DMF mixture. To that, 2,2'-bipyridine (1 mmol, 0.156 g) in 10 mL methanol was added. It was followed by the addition of copper acetate (1 mmol, 0.199 g) in 5 mL methanol. The resultant mixture was then further refluxed for about 4 h and allowed to cool. Dark green-colored block-shaped crystals were formed over a period of 7 days, which were then washed with methanol and dried in air.

Yield: 0.497 g (78%). Molar conductance ( $10^{-3}$  M DMF):  $10 \Omega^{-1}cm^2mol^{-1}$ . Anal. Calc. for  $C_{27}H_{30}N_6Cl_2CuO_2S$  ( $637.08 g mol^{-1}$ ): C, 50.90; H, 4.75; N, 13.19; S, 5.09. Found: C, 50.98; H, 4.70; N, 13.21; S, 5.03.

**SCHEME 2** The synthesis scheme for Complexes **1** and **2**



**SCHEME 3** The synthesis scheme for Complex **3**



## 2.4 | Physical measurements

Carbon, hydrogen, nitrogen, and sulfur analyses were carried out using a Vario EL III CHNS analyzer. Infrared spectra of the compounds were recorded on a JASCO FT-IR-5300 Spectrometer in the 4,000–400  $\text{cm}^{-1}$  range using KBr pellets. Electronic spectra were recorded on Thermo Scientific Evolution 220 model UV-Visible spectrophotometer in the 200–1,000 nm range using solutions in DMF. Diffuse reflectance spectroscopy (DRS) of the compounds was performed using an Ocean Optics USB-4000. Barium sulfate ( $\text{BaSO}_4$ ) powder was used as a background and standard reference during sample preparation. Molar conductivities of the complexes in DMF solutions ( $10^{-3}$  M) at room temperature were measured using a Systronic model 303 direct reading conductivity meter. Proton nuclear magnetic resonance ( $^1\text{H}$  NMR) spectra of the thiosemicarbazone and Zn(II) complex were recorded using Bruker AMX 400 FT-NMR Spectrometer with deuterated dimethylsulfoxide ( $\text{DMSO}-d_6$ ) as the solvent and TMS as the internal standard.

## 2.5 | X-ray crystallography

Single crystal X-ray diffraction experiments for the complexes were performed on a Bruker SMART APEXII CCD diffractometer, equipped with a graphite crystal, incident-beam monochromator, and a fine focus sealed tube with Mo  $K\alpha$  ( $\lambda = 0.71073$  Å) radiation as the X-ray source. The unit cell dimensions were measured, and the data collection was performed at 292[2] K. The programs APEX2 and SAINT were used for cell refinement, and SAINT and XPREP were used for data reduction.<sup>[11]</sup> Absorption corrections were carried out using SADABS based on Laue symmetry using equivalent reflections.<sup>[12]</sup> The structures were solved by direct methods and refined by full-matrix least-squares refinement on  $F^2$  using SHELXL-2014/7<sup>[13]</sup> provided in WinGX.<sup>[14]</sup> The molecular and crystal structures were plotted using DIAMOND version 3.2g<sup>[15]</sup> and ORTEP.

An outline of the information and crystallographic parameters of the complexes are given in Table 1. In the Cu(II) and Zn(II) complexes, anisotropic refinements were performed for all non hydrogen atoms, and all H atoms on C were placed in calculated positions, guided by difference maps, with C–H bond distances of 0.93–0.96 Å. H atoms were assigned as  $U_{\text{iso}} = 1.2U_{\text{eq}}$  (1.5 for Me). The hydrogen atoms attached to N(3) for **1** and **2** were located from difference maps, and N–H distances were restrained using DFIX instruction to possess a particular target value. The values (2 0 0), (1 0 0), (0 1 1),

**TABLE 1** Crystallographic data and structure refinement for Complexes **1** and **2**

Parameters	Complex 1	Complex 2
Empirical formula	$\text{C}_{29}\text{H}_{24}\text{Cl}_2\text{N}_6\text{O}_2\text{SZn}$	$\text{C}_{29}\text{H}_{24}\text{Cl}_2\text{CuN}_6\text{O}_2\text{S}$
Formula weight	656.87	655.04
Crystal, system, space group	Monoclinic, $P2_1/c$	Monoclinic, $P2_1/c$
Unit cell dimensions		
$a$ (Å)	21.5125(14)	21.703(4)
$b$ (Å)	13.8306(9)	13.744(2) Å
$c$ (Å)	9.6840(6)	9.7101(17) Å
$\alpha$ (°)	90	90
$\beta$ (°)	91.929(3)	91.896(8)
$\gamma$ (°)	90	90
Volume (Å <sup>3</sup> )	2879.7(3)	2894.8(8)
$Z$	4	4
Calculated density (mg/m <sup>3</sup> )	1.515	1.503
Absorption coefficient, $\mu$ (mm <sup>-1</sup> )	1.150	1.050
$F(000)$	1,344	1,340
$\theta$ range for data collection	2.400° to 28.313°	2.392° to 28.253°
Limiting indices	$-28 \leq h \leq 27,$ $-18 \leq k \leq 16,$ $-12 \leq l \leq 12$	$-28 \leq h \leq 28,$ $-18 \leq k \leq 12,$ $-12 \leq l \leq 12$
Reflections collected	34,693	23,162
Unique reflections ( $R_{\text{int}}$ )	7,167 [R (int) = 0.0389]	7,163 [R (int) = 0.0975]
Completeness to $\theta$	25.242(99.9%)	25.242(99.9%)
Max. and min. transmission	0.8030 and 0.7740	0.8030 and 0.7740
Goodness-of-fit on $F^2$	1.019	0.936
Final $R$ indices [ $I > 2\sigma(I)$ ]	$R_1 = 0.0376,$ $wR_2 = 0.0827$	$R_1 = 0.0518,$ $wR_2 = 0.0915$
$R$ indices (all data)	$R_1 = 0.0663,$ $wR_2 = 0.0934$	$R_1 = 0.1492,$ $wR_2 = 0.1191$
Largest diff. peak and hole	0.419 and $-0.386$	0.301 and $-0.457$

$$R_1 = \frac{\sum ||F_o| - |F_c||}{\sum |F_o|} \quad wR_2 = \left[ \frac{\sum w(F_o^2 - F_c^2)^2}{\sum w(F_o^2)^2} \right]^{1/2}$$

and (1 1 0) in Complex **1** and (2 0 0), (1 0 0) and (1 1 0) in Complex **2** are omitted due to bad agreement.

## 2.6 | Computational methodology

Density functional theory (DFT) calculations were carried out using the Gaussian09<sup>[16]</sup> package at DFT based on the B3LYP/LANL2DZ basis set. The optimized structure was visualized using Chemcraft version 1.6 package. The highest occupied molecular orbital energy ( $E_{\text{HOMO}}$ ), the lowest unoccupied molecular orbital energy ( $E_{\text{LUMO}}$ ) and HOMO–LUMO energy gap ( $\Delta E$ ) for the complexes were calculated, and with the help of those values, different quantum chemical parameters were also studied.

Electrostatic potential (ESP) colored molecular surface map with ESP surface extrema *via* VMD based on the data outputted by Multiwfn is plotted.<sup>[17]</sup> A blue–white–red color code is employed, where the blue is used for an electropositive region, white for neutral, and red for an electronegative region.

## 2.7 | Molecular docking study

The molecular docking studies were performed using Auto Dock Tools (ADT) and AutoDock vina. The cif format files were converted to pdb files using Mercury software. The crystal structure of the B-DNA dodecamer d(CGCAAATTTTCGC)<sub>2</sub> (PDB ID: 1BNA) was downloaded from the protein data bank.<sup>[18,19]</sup> Outputs of the docked poses were exported to Discovery Studio for visual inspection of the binding modes and for the probable polar and hydrophobic interactions of the complexes with DNA. The results were visualized using VMD software.

## 2.8 | DNA binding studies

The binding affinity between the complexes and DNA was studied in Tris–HCl buffer (pH: 7.4) at room temperature. Absorption spectroscopy was used to determine the concentration of DNA per nucleotide. An absorption titration experiment with a fixed concentration of complex (25  $\mu\text{M}$ ) with a gradually increasing concentration of CT-DNA (8.6 to 86  $\mu\text{M}$ ) was performed. An identical quantity of CT-DNA is supplied to both the test and reference solution while measuring the absorbance to eliminate the absorbance of CT-DNA itself. From the absorption spectral titration data, the binding constant  $K_b$  for the interaction of complex was calculated by the equation

$$\frac{[\text{DNA}]}{[\epsilon_a - \epsilon_f]} = \frac{[\text{DNA}]}{[\epsilon_b - \epsilon_f]} + \frac{1}{K_b([\epsilon_b - \epsilon_f])}$$

The apparent extinction coefficient  $\epsilon_a$  corresponds to  $A_{\text{obs}}/([M])$ ,  $\epsilon_f$  is the extinction coefficient of the free compound and  $\epsilon_b$  is the extinction coefficient of the compound when it is fully bound to DNA. Now, a plot of  $([\text{DNA}])/((\epsilon_a - \epsilon_f))$  against  $[\text{DNA}]$  is drawn; the slope of the plot corresponds to  $1/((\epsilon_b - \epsilon_f))$ , and the intercept corresponds to  $1/(K_b(\epsilon_b - \epsilon_f))$ . Thus, the binding constant of  $K_b$  is the ratio of the slope to the intercept. The mode of binding between the CT-DNA and complexes was also examined using fluorescence spectral titration. It is recorded at room temperature. Ethidium bromide (EB) is used as a standard intercalator. The EB intercalates with CT-DNA, resulting in high fluorescence, which further reduces by the addition of the complexes. The fluorescence quenching can be explained via the Stern–Volmer equation:

$$\frac{F_0}{F} = 1 + K_q [Q]$$

$K_q$  is the linear Stern–Volmer quenching constant, and the concentration of the complex is represented by  $[Q]$ .  $F_0$  and  $F$  are the fluorescence intensity in the absence and presence of the complex, respectively. The slope of the plot of  $F_0/F$  against  $[Q]$  gave the quenching constant,  $K_q$ .

## 2.9 | Agarose gel electrophoresis

In the gel electrophoresis experiments, supercoiled PTZ57R plasmid DNA dissolved in Tris HCl buffer (7.2) was treated with metal complexes and made up to 10  $\mu\text{L}$  using nuclease-free water, and the mixture was incubated at 37 °C for 24 h. Each sample was loaded into a 1% agarose gel. Electrophoresis was taken for 1 h at 40 V in 1XTAE buffer. Then, the gel is visualized under UV light. The cleavage result was calculated using the Biorad Geldoc software version 4.1.

## 2.10 | Cytotoxicity evaluation by the MTT assay

The MDA-MB-231 cell line was initially procured from the National Centre for Cell Sciences (NCCS), Pune, India and maintained in Dulbecco's modified Eagles medium (DMEM) Himedia. The cell line was cultured in 25  $\text{cm}^2$  tissue culture flask with DMEM supplemented with 10% fetal bovine serum (FBS), L-glutamine, sodium

bicarbonate and an antibiotic solution containing penicillin (100 U/mL), streptomycin (100 µg/mL), and amphotericin B (2.5 µg/mL). Cultured cell lines were kept at 37 °C in a humidified 5% CO<sub>2</sub> incubator. The viability of cells was evaluated by direct observation of cells by an inverted phase-contrast microscope and followed by the MTT assay method.

### 2.10.1 | Antiproliferative effect by MTT method

Fifteen milligrams of MTT (Himedia, M-5655) was reconstituted in 3 mL phosphate-buffered saline (PBS) until completely dissolved and sterilized by filter sterilization. After 24 h of the incubation period, the sample content in wells was removed, and 30 µL of the reconstituted MTT solution was added to all test and control wells. It was gently shaken well and then incubated at 37 °C in a humidified 5% CO<sub>2</sub> incubator for 4 h. After the incubation period, the supernatant was removed and 100 µL of the MTT solubilization solution (DMSO) was added and the wells were mixed gently by pipetting up and down to solubilize the formazan crystals. The absorbance values were measured by using a microplate reader at a wavelength of 570 nm and the percentage viability is calculated as below.

$$\% \text{viability} = \frac{\text{Mean OD samples} \times 100}{\text{Mean OD of the control group}}$$

## 3 | RESULTS AND DISCUSSION

The complexes are soluble in DMF and DMSO and are nonelectrolytes in nature ( $5\text{--}10 \Omega^{-1}\text{cm}^2\text{mol}^{-1}$ ).<sup>[20]</sup>

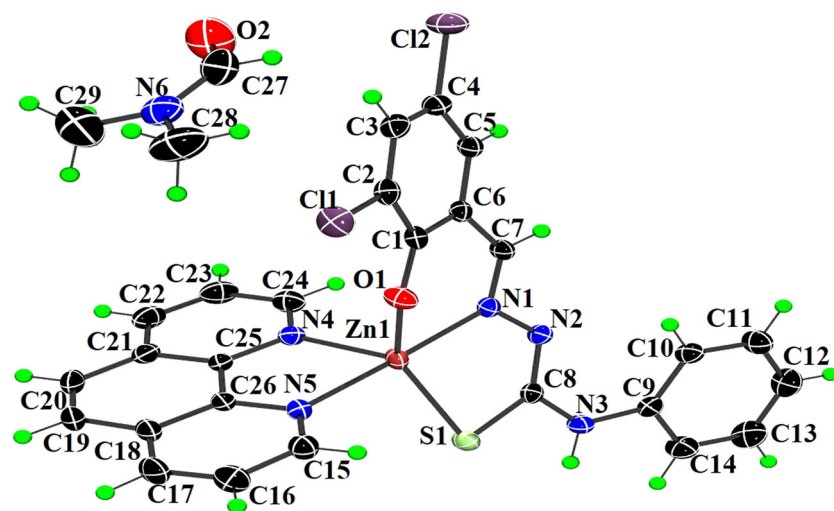


**FIGURE 1** Oak Ridge Thermal Ellipsoid Plot (ORTEP) of [Zn(dspt)(phen)]·DMF (**1**). Displacement ellipsoids are drawn with 30% probability

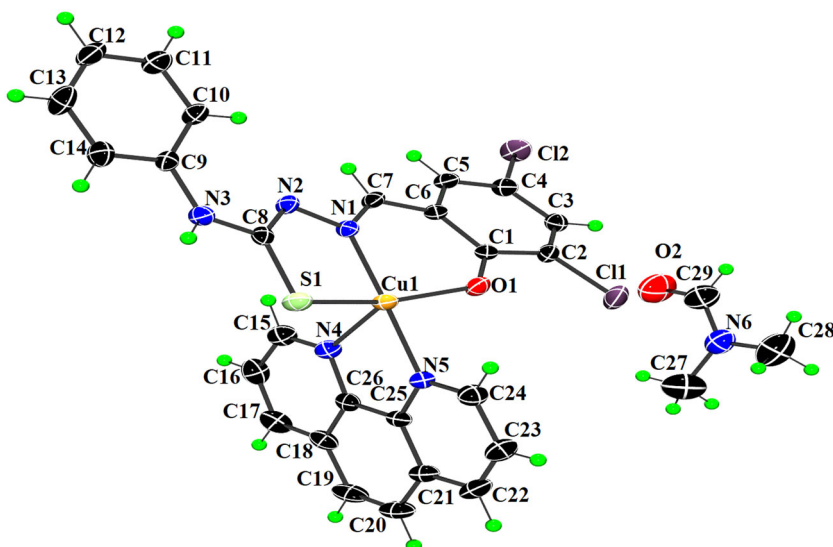
The thiosemicarbazones and their complexes were characterized by infrared (IR), <sup>1</sup>H NMR, and UV–Visible spectroscopic techniques and single-crystal X-ray diffraction studies. IR, UV spectra and single-crystal details of Complex **3** are the same as reported by us.<sup>[10]</sup>

### 3.1 | Description of crystal structures

The single crystals of complexes appropriate for X-ray diffraction studies were acquired from DMF at room temperature. Coordination to the metal ions lengthens the C–S bond substantially to 1.73 Å (**1**), 1.737(4) Å (**2**) from 1.680 Å in unsubstituted salicylaldehyde-N<sup>4</sup>-phenylthiosemicarbazone,<sup>[21]</sup> as expected on coordination to thiolate sulfur.

Selected bond lengths and bond angles are summarized in Table S1. The ORTEP diagrams of the compounds along with the atom numbering scheme are given in Figures 1 and 2. Complexes **1** and **2** got crystallized in the monoclinic *P*<sub>2</sub><sub>1</sub>/*c* space group. The central atom (Zn/Cu) in the complex is coordinated by phenolate oxygen (O(1)), azomethine nitrogen (N(1)), thiolato sulfur (S(1)) of the thiosemicarbazone, and the pyridine nitrogen (N(4) and N(5)) of bipyridine and 1,10-phenanthroline derivative, respectively. DMF molecule is present outside the coordination sphere. The geometry of the complexes is derived from the trigonality index,  $\tau_5 = ((\beta - \alpha))/60$ , where  $\beta$  and  $\alpha$  are the greatest basal angles.<sup>[22]</sup> The  $\tau_5$  value for Compound **1** is 0.55, indicating that it exhibits a distorted trigonal bipyramidal geometry, whereas Complex **2** has  $\tau_5 = 0.28$ , which exhibits a distorted square pyramidal geometry.<sup>[21]</sup> The ONS donor atoms of thiosemicarbazones occupy the upper plane, and the NN-donor heterocyclic bases exhibit pivotal central restricting mode, that is, axial–equatorial binding mode. The dianionic form of the

**FIGURE 2** Oak Ridge Thermal Ellipsoid Plot (ORTEP) of  $[\text{Cu}(\text{dspt})(\text{phen})]\cdot\text{DMF}$  (**2**). Displacement ellipsoids are drawn with 30% probability



thiosemicarbazones occurring due to the enolization of the  $-\text{NH}-\text{C}(=\text{S})-\text{NHPH}$  moiety to  $-\text{N}=\text{C}(-\text{SH})-\text{NHPH}$  and phenolic  $-\text{OH}$ , eventually resulting in the  $\pi$ -conjugation in the planar structure, which encourages its equatorial binding. Thus, heterocyclic bases adopt axial-equatorial binding. The results are different as compared to that of the binding of monoanionic ONS donor ligands that are reported.<sup>[23]</sup> The C(7)–N(1) and N(2)–C(8) distances are comparable with that of C=N bond length. The N(1)–N(2) bond lengths in both compounds are larger due to extensive conjugation of the ligand on complex formation. The Cu(1)/Zn(1)–N(3) bond lengths are shorter as compared with the Cu/Zn–N bond lengths of bipyridine and phenanthroline, which indicate that the thiosemicarbazone moiety dominates equatorial bonding. Restricted bite angles imposed by thiosemicarbazone and heterocyclic bases can be the reason for the deviation from a perfect geometry. The Cu–N bond lengths of the heterocyclic bases are longer than those reported for mononuclear copper(II)/zinc (II) complexes, indicating a weaker binding of the bases compared with the thiosemicarbazone.<sup>[22,23]</sup>

### 3.2 | Supramolecular interaction

The packing of molecules in the crystal lattice is stabilized by hydrogen bonding,  $\pi \cdots \pi$ , and C–H $\cdots\pi$  interactions (Tables S2–S5). The crystal structure of Complex **1** displays intermolecular and intramolecular interactions. Three prominent  $\pi \cdots \pi$  interactions are observed among Cg(8) $\cdots$ Cg(4), Cg(5) $\cdots$ Cg(8) and Cg(4) $\cdots$ Cg(5) at distances of 3.70, 3.68, and 3.79 Å, respectively (Figure 3). An appreciable C–H $\cdots\pi$  interaction is observed between C(19)–H(19) and Cg(6) at a H(19) $\cdots$ Cg(6) distance of 2.66 Å (Figure 3). The oxygen

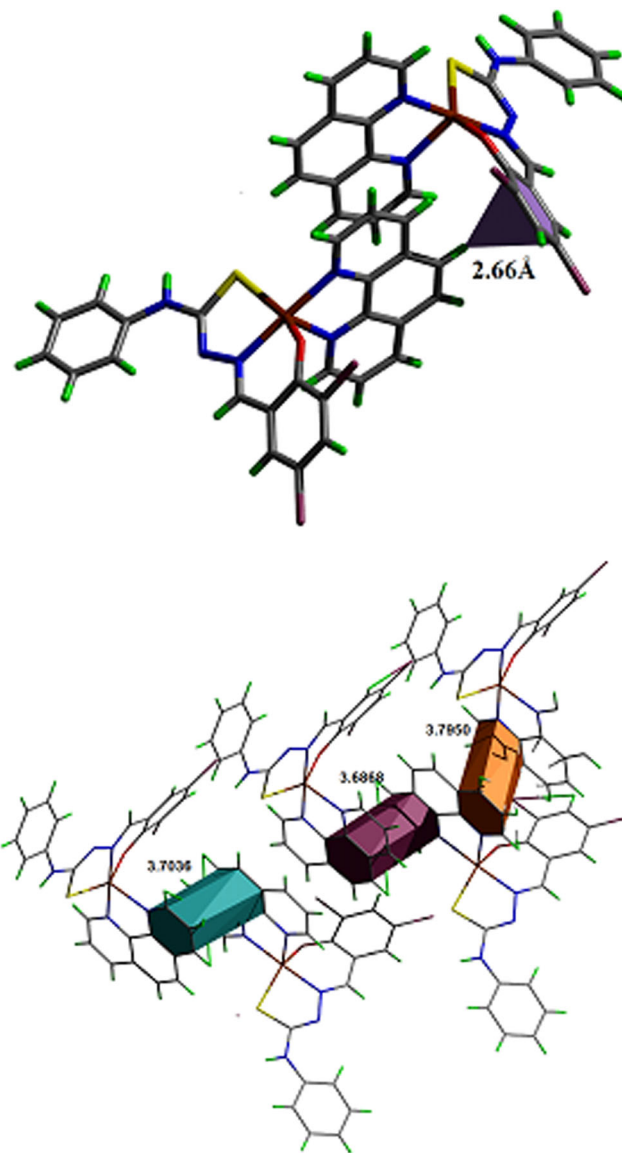


**FIGURE 3** C–H $\cdots\pi$  and  $\pi \cdots \pi$  interactions in  $[\text{Zn}(\text{dspt})(\text{phen})]\cdot\text{DMF}$  (**1**)

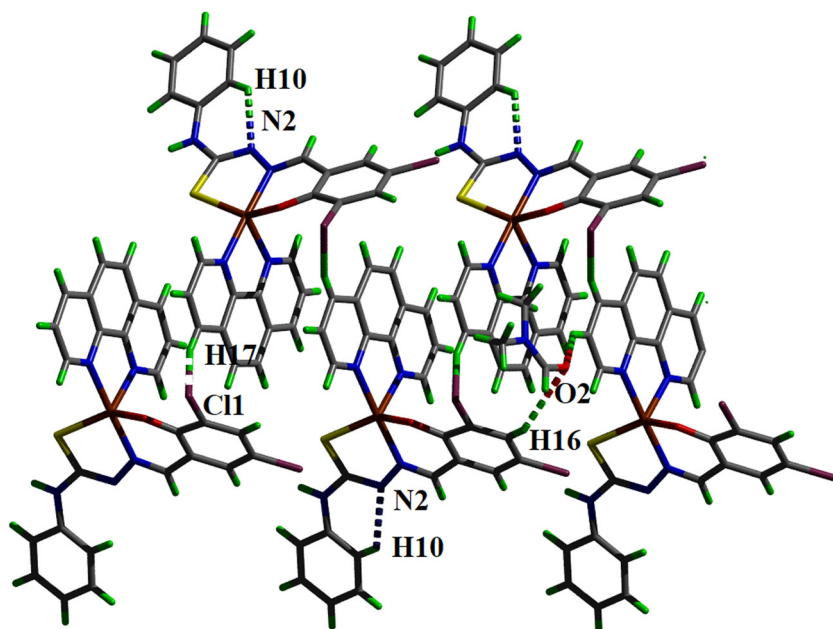


**FIGURE 4** Hydrogen bonding interactions present in  $[\text{Zn}(\text{dspt})(\text{phen})]\cdot\text{DMF}$  (1)

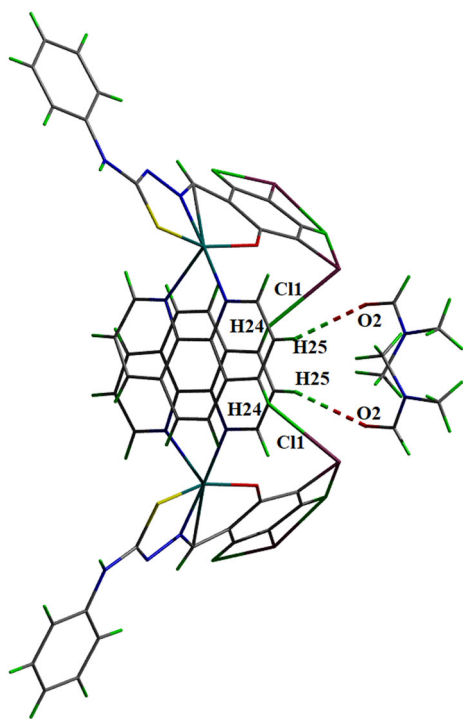


**FIGURE 5** Hydrogen bonding interactions in  $[\text{Cu}(\text{dspt})(\text{phen})]\cdot\text{DMF}$  (2)

atom of DMF acts as an acceptor to form hydrogen bond with  $\text{C}(16)\cdots\text{H}(16)$  at a distance of 2.48 Å. Other hydrogen bonding interactions are  $\text{Cl}(1)$  to the bipyridine ring  $\text{C}(17)\cdots\text{H}(17)$  with a distance of 2.78 Å, benzene ring  $\text{C}(10)\cdots\text{H}(10)$  is interacting with  $\text{N}2$  at a distance of 2.32 Å (Figure 4).

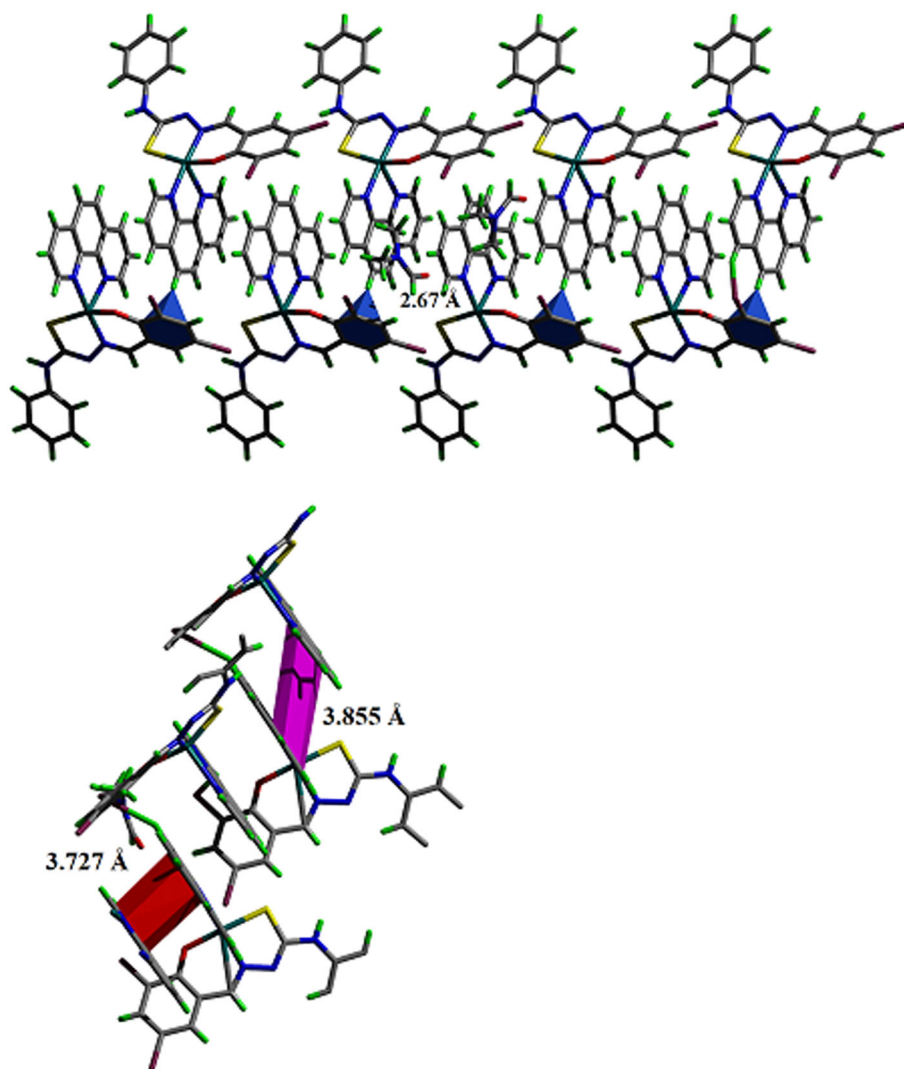
In Complex 2, the solvent DMF molecule makes a hydrogen bonding interaction with  $\text{C}(25)\text{--}\text{H}(25)\cdots\text{O}$  (2) and another hydrogen bonding  $\text{C}(24)\text{--}\text{H}(24)\cdots\text{Cl}$  (1) with  $\text{D}\cdots\text{A}$  distances of 2.46 and 2.82 Å, respectively (Figure 5). One  $\text{C}\text{--}\text{H}\cdots\pi$  interaction of the type  $\text{C}(21)\text{--}\text{H}(21)\cdots\text{Cg}(6)$  with  $\text{H}\cdots\text{Cg}$  distance 2.67 Å is also present in the molecule, where  $\text{Cg}(6)$  is the ring comprising of atoms  $\text{C}(1)\text{--}\text{C}(2)\text{--}\text{C}(3)\text{--}\text{C}(4)\text{--}\text{C}(5)\text{--}\text{C}(6)$  (Figure 6).

### 3.3 | IR spectra

The IR spectra of  $\text{H}_2\text{dspt}$  and its complexes were recorded. The appearance of the bands around the  $3,470\text{ cm}^{-1}$  region confirmed the presence of hydroxyl groups in the thiosemicarbazone. A band at  $1,298\text{ cm}^{-1}$  for  $\text{H}_2\text{dspt}$  was assigned to  $\text{C}\text{--}\text{O}$  stretching vibration. The azomethine stretching vibration  $\nu(\text{C}=\text{N})$  appeared at  $1,638\text{ cm}^{-1}$ . The bands corresponding to  $\nu(\text{C}=\text{S})$  were detected around  $1,275\text{ cm}^{-1}$  for the ligand. Further, the appearance of the band in the  $1,110\text{ cm}^{-1}$  region indicates the presence of  $\nu(\text{N}\text{--}\text{N})$  stretching frequency. Hence, the IR spectrum of the proligand is confirmed.<sup>[24]</sup>

The IR spectra of the complexes were studied to understand the binding of a tridentate ligand to the metal center. The absence of the band corresponding to the  $\text{O}\text{--}\text{H}$  stretching frequency for the thiosemicarbazone shows the deprotonation of a hydroxyl group and participation of oxygen in coordination with the metal. The bands corresponds to  $\nu(\text{C}=\text{N})$  and  $\nu(\text{C}\text{--}\text{S})$  are slightly shifted to lower wavenumbers for the complexes. The increase in the frequency of  $\nu(\text{N}\text{--}\text{N})$  band in the spectra of the

**FIGURE 6** C–H... $\pi$  and  $\pi$ – $\pi$  interactions in [Cu(dspt)(phen)]·DMF (2)



complexes due to the increase in the bond strength again confirms the coordination *via* the azomethine nitrogen. Thus, the IR data confirm the formation of the complex and its ONS donor behavior.<sup>[25]</sup> IR spectral assignments of thiosemicarbazone and complexes are tabulated in Table S6.

### 3.4 | Electronic spectra

The electronic spectra of the complexes are recorded in DMF solution ( $1 \times 10^3$  M) (Table S7 and Figures S1 and S2). The absorption bands in the range of 260 ( $24,090 \text{ } \epsilon/\text{M}^{-1} \text{ cm}^{-1}$ ) and 320 nm ( $9,240 \text{ } \epsilon/\text{M}^{-1} \text{ cm}^{-1}$ ) for  $\text{H}_2\text{dspt}$  have been attributed to  $\pi \rightarrow \pi^*$  and  $n \rightarrow \pi^*$  transitions. The spectra of complexes showed two bands at the 320–330 nm range, which were allocated to  $\pi \rightarrow \pi^*$  and  $n \rightarrow \pi^*$  excitations, respectively, of ligands. The bands have slightly higher wavelengths as a result of complexation. The complexes also exhibited charge transfer bands

in the 410–420 nm range. For Complex **2**, a broad peak around 570 nm ( $25,700 \text{ } \epsilon/\text{M}^{-1} \text{ cm}^{-1}$ ) is characteristic of the  $d-d$  transition ( $1 \times 10^5$  M).<sup>[26,27]</sup> Diffuse reflectance spectroscopy of complexes were also taken, and results were comparable and are given in Figures S3–S5 (Table S8).

### 3.5 | $^1\text{H}$ NMR spectra

The  $^1\text{H}$  NMR spectra of the proligand,  $\text{H}_2\text{dspt}$ , and its complexes were recorded with  $\text{DMSO-}d_6$  as the solvent and trimethylsilane (TMS) as the internal standard. The  $^1\text{H}$  NMR spectrum of the proligand  $\text{H}_2\text{dspt}$  is compared with that of Complex **1**. The peaks of the –OH proton (11.8 ppm) and –NH (10.2 ppm) protons of the ligand disappear on complexation in Complex **1**. The peak around 9 ppm represents –CH=N peak. The low field position of  $^{-4}\text{NH}$  around 7.16 ppm could be attributed to the deshielding caused by the phenyl group and the adjacent

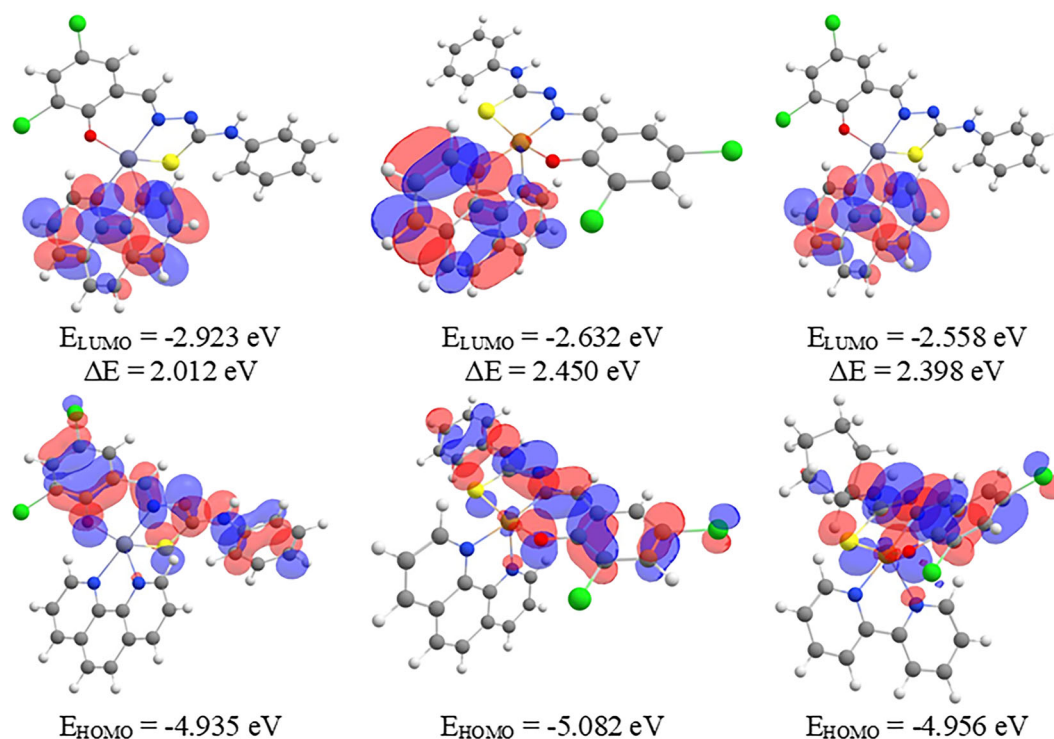


**FIGURE 7** Frontier orbitals of Complexes **1**, **2**, and **3** along with their associated energies

$-\text{N}=\text{C}<$  of the system  $-\text{N}=\text{C}(\text{SH})-\text{NH}-\text{C}_6\text{H}_5$ . These results indicate that the coordination is *via* deprotonation of ONS donor ligand through iminolic nitrogen and phenolic oxygen. This provides evidence for the coordination of thiolato sulfur through iminolization after deprotonation.<sup>[28]</sup>

### 3.6 | DFT study

To understand the electronic transitions occurring in the complexes, DFT calculations were carried out using B3LYP/LANL2DZ basis set using the Gaussian 09 program. The main orbitals that take part in chemical reactions are called the frontier molecular orbitals (FMOs) (Figure 7). HOMO, the highest occupied molecular orbital, behaves as an electron donor, while LUMO, the lowest unoccupied molecular orbital, behaves as an electron acceptor. Localization of HOMO in all these complexes is in the ligand moiety and LUMO localizes in the base region. Molecular chemical stability is indicated by the energy gap between the HOMO and LUMO. Many properties like chemical reactivity, kinetic stability, optical polarizability, chemical hardness, softness, and electronegativity can be determined by the help of the energy gap between HOMO and LUMO (Table 2).

To get an idea about the in-depth analysis of the electronic differences in these complexes, molecular ESPs were mapped on the electron density surface (Figure 8).

The map shows the information about the charge distribution of a molecule because of the properties of the nucleus and the nature of ESP energy. With the help of color coding, we can visualize the molecular shape and ESP. The red region indicates a highly negative potential and the blue region indicates a positive ESP. It indicates that the red color region will have an electrophilic attack and the blue color region will have a nucleophilic attack. The ESP plot clearly indicates the difference in the presence of cyclohexyl ring in Complex **3** as compared with the phenyl ring in Complexes **1** and **2**. The maximum negative ESP is on the base containing region and the positive potential is on the ligand moiety.

### 3.7 | Molecular docking with DNA

Molecular docking is an important *in silico* computational tool for the design of new chemotherapeutic drugs,

**TABLE 2** Global chemical reactivity descriptors for Compounds **1**, **2**, and **3**

	<b>1</b>	<b>2</b>	<b>3</b>
Electronegativity	3.929	3.857	3.757
Chemical hardness	1.006	1.225	1.199
Chemical potential	-3.929	-3.857	-3.757
Chemical softness	0.497	0.408	0.416
Electrophilicity index	7.672	6.071	5.885

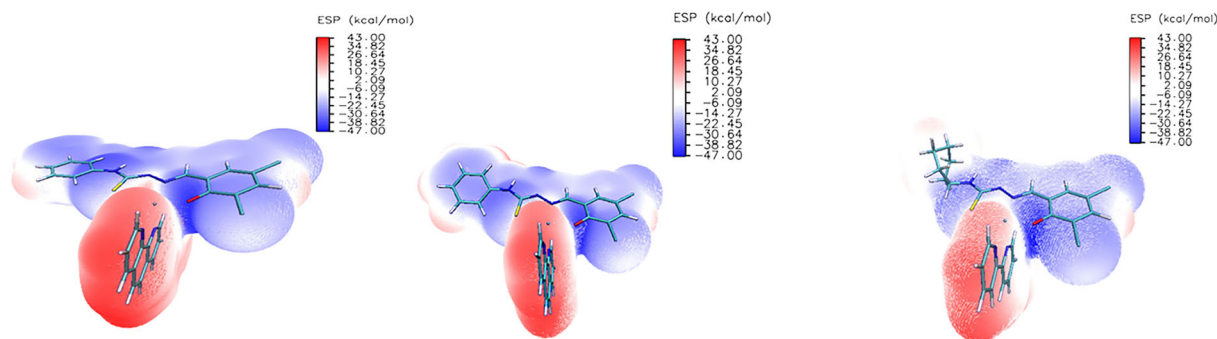


**FIGURE 8** Molecular electrostatic potential maps for Complexes 1–3

**TABLE 3** Docking interactions of the compounds with 1BNA

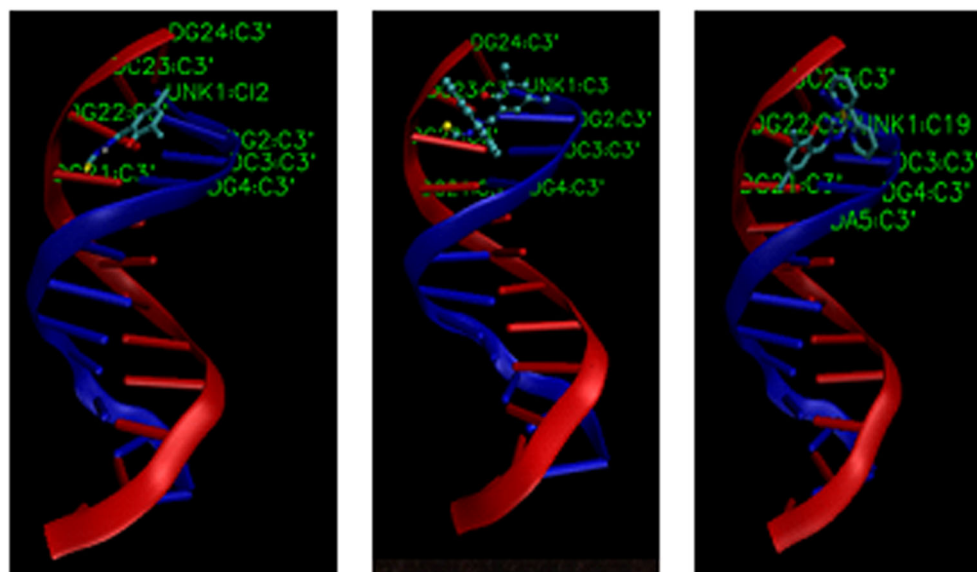
Compound	Docking score (kcal/mol)	Hydrogen bonding interaction	Electrostatic/hydrophobic interactions
1	−8.4	G4(H9):N2 G22(O4'):H3'	A6:O1
2	−8.6	C23(O4'):H3'	C21:O2 G4:N3
3	−8.4	C23(O3'):C24	G4:N3 C21:O2

which foresees various noncovalent interactions present between the drug molecule and the nucleic acids of DNA. To get an insight into the preferred mode of binding and to understand the drug molecule-biomolecule interaction, the docking technique is adopted. Energy, hydrogen bonding and hydrophobic interactions between complexes and DNA were analyzed by the different conformation of the docked complexes. The docking score and various interactions are shown in Table 3.

The docking results shows that the DNA binds comfortably with the complexes with various interactions like van der Waals interaction, hydrophobic and hydrogen

bonding contacts (Figure 9). The complexes were subjected to molecular docking with the crystal structure of the B-DNA dodecamer d (CGCAAATTCGC)<sub>2</sub> with PDB ID:1BNA using Auto Dock. The binding energy of Complexes 1–3 are −8.4, −8.6, and −8.4 kcal mol<sup>−1</sup>. Molecular docking studies of the complexes with B-DNA dodecamer reveal that the docked Complex 2 can bind more efficiently to the DNA molecule and can be a potential scaffold to be used for therapeutic purposes. The presence of phenanthroline and bipyridine moiety in these complexes enriches the hydrophobic interactions with the base pairs of DNA.<sup>[29,30]</sup> Thus, it can be a promising DNA-targeting anticancer drug.

**FIGURE 9** Molecular docking interaction of Complexes 1–3 with 1-BNA



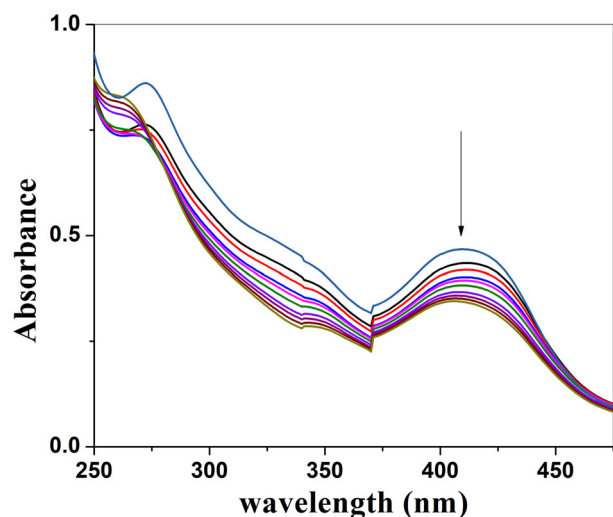


**FIGURE 10** Absorption titration of Complex 1 (25  $\mu\text{M}$ ) with different concentrations (8.6–86  $\mu\text{M}$ ) of CT-DNA

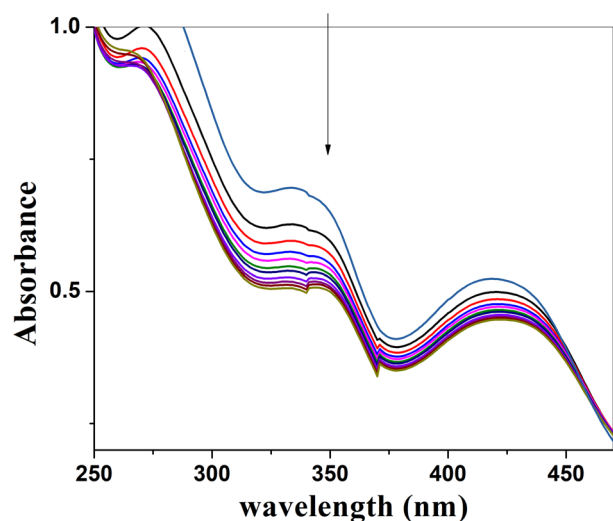


**FIGURE 11** Absorption titration of Complex 2 (25  $\mu\text{M}$ ) with different concentrations of CT-DNA (8.6–86  $\mu\text{M}$ )

### 3.8 | DNA binding

The transition metal complexes can bind to DNA *via* covalent or noncovalent interactions. A nitrogen base of DNA, for example, guanine N7, can be replaced by the labile ligand and is termed as a covalent interaction. Noncovalent interactions comprise of intercalation and electrostatic or groove binding.<sup>[31]</sup> In these complexes, we see an intercalative mode of binding.<sup>[32]</sup> The intercalative mode is confirmed by the notable decrease in the intensity and the shift of electronic spectral bands. This can be due to the stacking interaction observed between the aromatic chromophore of the complexes and DNA base pairs. The strength of intercalative interaction depends

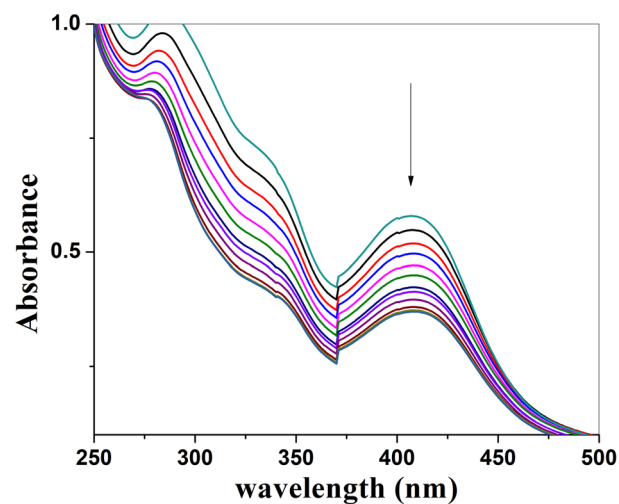


**FIGURE 12** Absorption titration of Complex 3 (25  $\mu\text{M}$ ) with different concentrations of CT-DNA (8.6–86  $\mu\text{M}$ )

**TABLE 4** CT-DNA binding constant ( $K_b$ ) from absorption spectroscopy, quenching constant ( $K_q$ ) values from fluorescence spectroscopy

Compound	$K_b$ ( $\text{M}^{-1}$ )	$K_q$ ( $\text{M}^{-1}$ )
1	$1.7 \times 10^4$	$4.6 \times 10^5$
2	$3.7 \times 10^4$	$4.7 \times 10^5$
3	$5 \times 10^3$	$4.1 \times 10^5$

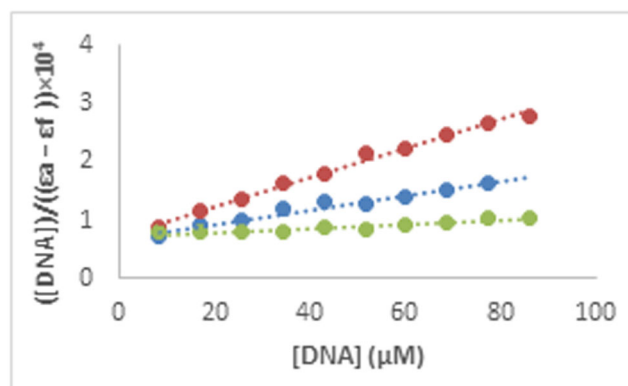


**FIGURE 13** Plot of  $[\text{DNA}]/(\epsilon_a - \epsilon_f)$  versus  $[\text{DNA}]$  for the titration of the complexes with CT DNA. (blue, 1; red, 2; and green, 3)

on the degree of hypochromism and the amount of shift.<sup>[33]</sup> A fixed amount (25  $\mu\text{M}$ ) of complexes was titrated with an increasing amount of CT-DNA, which ranges from 8.6–86  $\mu\text{M}$ . Intraligand transitions are observed at about 246 nm and metal-to-ligand transitions are observed at around 403 nm. The absorption spectra shows that as the amount of DNA is increased, a

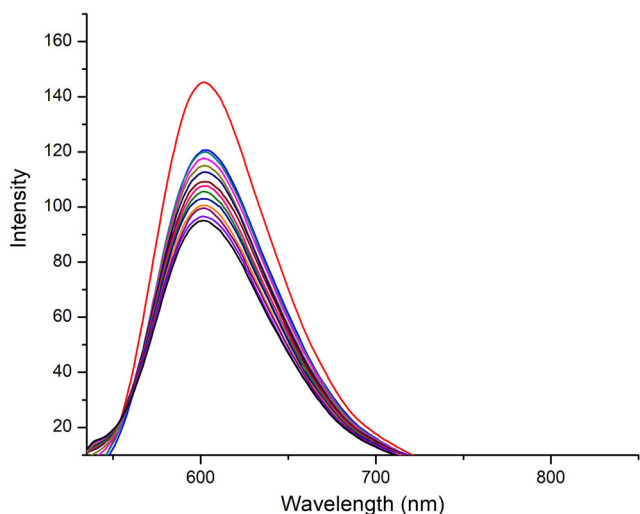


**FIGURE 14** Fluorescence quenching curves of ethidium bromide (EB) bound to DNA (86  $\mu\text{M}$ ) with different concentrations of Complex 1 (0.5–5  $\mu\text{M}$ )

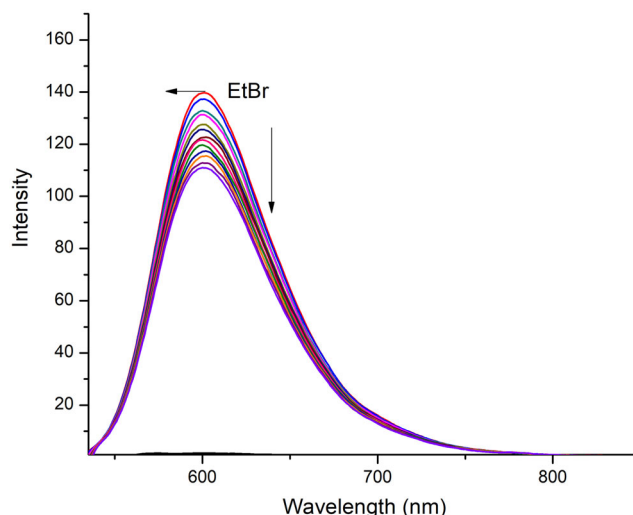


**FIGURE 16** Fluorescence quenching curves of ethidium bromide (EB) bound to DNA (86  $\mu\text{M}$ ) with different concentrations of Complex 3 (0.5–5  $\mu\text{M}$ )

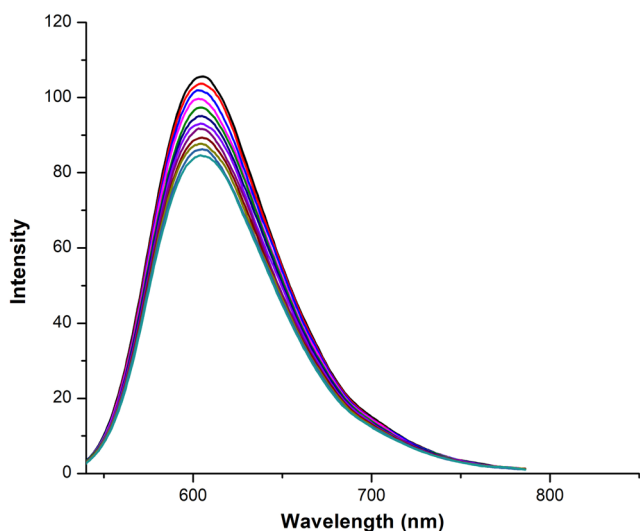


**FIGURE 15** Fluorescence quenching curves of ethidium bromide (EB) bound to DNA (86  $\mu\text{M}$ ) with different concentrations of Complex 2 (0.5–5  $\mu\text{M}$ )

significant hypochromism is observed (Figure 10–12) and the binding constants ( $K_b$ ) thus determined are tabulated in Table 4. The observed values of  $K_b$  revealed that the complexes bound to DNA are relatively stronger (Figure 13).

In the present study, the mode of binding of complexes and DNA was ascertained by the EB displacement by fluorescence emission spectral studies.<sup>[34]</sup> An increasing amount of complexes with DNA pretreated with EB causes an appreciable decrease in emission intensity, thereby indicating the replacement of EB by the complexes (Figures 14–16). These observations suggest that

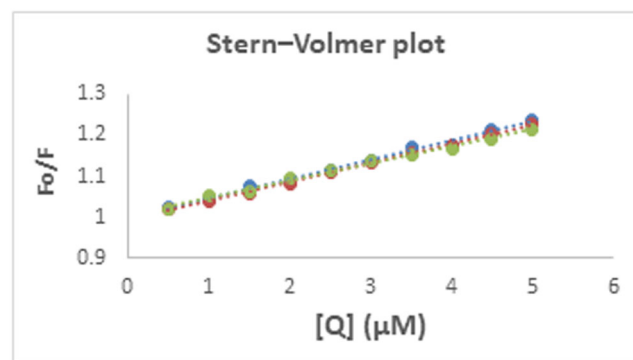


**FIGURE 17** Plot of Stern–Volmer plot of fluorescence titrations of the complexes with CT DNA. (1, blue; 2, orange; and 3, green)

complexes bind to DNA *via* intercalative mode.<sup>[33]</sup> In both complexes, the Stern–Volmer plot was found to be linear, and the Stern–Volmer constant is higher (Figure 17). The  $K_b$  and  $K_q$  values are tabulated in Table 4. The value shows that the binding ability of the three complexes with CT-DNA follows the order  $2 > 1 > 3$ .

### 3.9 | DNA cleavage

To explore the DNA cleavage ability of Complexes 1–3, PTZ57R DNA (2,886 base pairs) was incubated at 37  $^{\circ}\text{C}$  in Tris–HCl buffer at pH 7.2 for 24 h in the absence of any external agent.<sup>[32]</sup> Complexes cleave SC (Form I) DNA into nicked circular (NC) (Form II) DNA moderately (Figure 18). At 4  $\mu\text{M}$ , the DNA cleavage efficiency

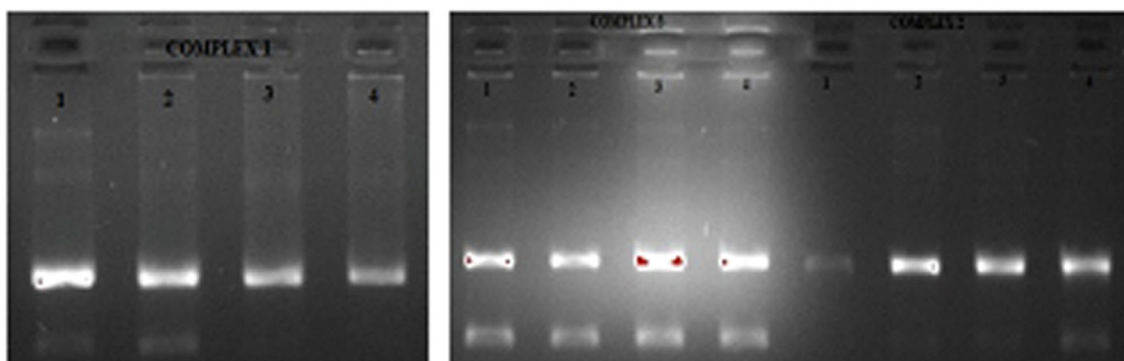


**FIGURE 18** Electrophoresis separations of PTZ57R DNA induced by complexes 1–3 (in 1, 2, 3, and 4  $\mu\text{M}$  concentrations, respectively)

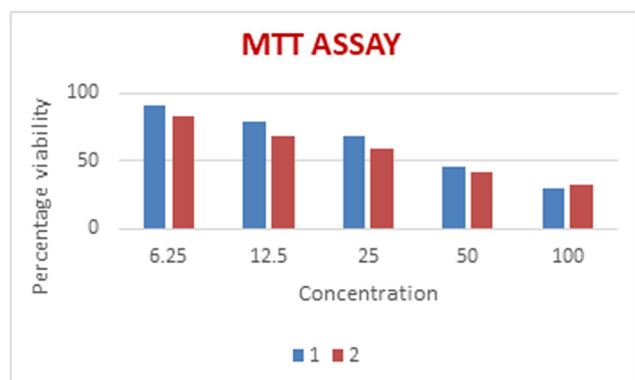


**FIGURE 19** Graphical representation of *in vitro* cytotoxicity result showed by the complexes

follows the order complex 3 > 2 > 1. The stability of DNA is controlled by the phosphodiester backbone.<sup>[35,36]</sup>

### 3.10 | *In vitro* cytotoxicity

The *in vitro* cytotoxicity of Complexes 1 and 2 was studied against a human breast cancer cell line (MD-

MBA-231)<sup>[37]</sup> (Figure 19). Complexes were dissolved in DMSO and a blank sample with the same volume of DMSO was taken as control. The results were analyzed by their  $\text{IC}_{50}$  value, that is, the cell inhibition value. The results showed that Complex 2 exhibited the highest inhibitory effect value of  $\text{IC}_{50} = 23.93 \mu\text{g/ml}$  as compared with Complex 1 ( $\text{IC}_{50} = 44.40 \mu\text{g/ml}$ ). Phase-contrast images are shown in Figure 20.

## 4 | CONCLUSION

Here, we have reported two novel and one already reported Cu(II) and Zn(II) complexes involving tridentate donor thiosemicarbazones. The complexes have been well characterized by spectroscopic techniques and single-crystal X-ray diffraction analysis. The difference in Complexes 1 and 2 is the metal atom present in the system with 1,10-phenanthroline acting as co-ligand and the third complex with a different thiosemicarbazone with 2,2'-bipyridine acting as the co-ligand. There are nice and significant C–H $\cdots\pi$ ,  $\pi\cdots\pi$  stacking, H-bonding interactions present in every molecule, which resulted in the stabilization

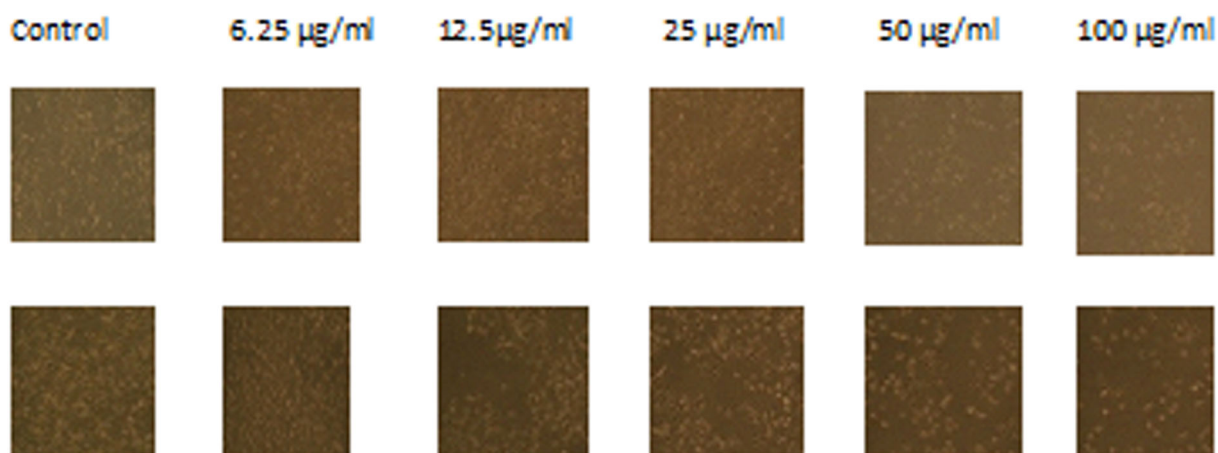


**FIGURE 20** Phase-contrast images of Complexes 1 and 2 at different concentrations

of the compounds. Analyses of frontier orbitals of the complexes were carried out. The DNA binding ability of the complexes was studied using absorbance and fluorescence spectroscopic technique. Complexes bind effectively to DNA in the order  $10^5 \text{ M}^{-1}$  through intercalative mode of binding. The DNA cleavage ability of the complexes showed that complexes cleaved DNA without an oxidizing agent. Further molecular docking confirmed the binding affinity of the complexes with DNA. It has been established that the total hydrophobicity of the ligand system directed by the substituent existing in the ligand part of the metal complex plays a critical role in the DNA binding, cleavage, and anticancer properties. Thus, when the base is a phen ring rather than a biphy ring, there is an enhancement in the DNA binding ability. The *in vitro* cytotoxicity of **1** and **2** complexes against a human breast cancer cell line (MD-MBA-231) exhibits lower antitumor activity for Complex **2** compared that of Complex **1**. This result agrees well with their DNA binding abilities. Thus, our complexes showed relevant biological activities targeting DNA and thus giving new potential anticancer drugs with useful reference.

#### ACKNOWLEDGEMENTS

Nimya Ann Mathews acknowledges the University Grants Commission, New Delhi, India, for the award of Senior Research Fellowship (UGC Ref No: 55/(CSIR-UGC NET JUNE 2017) dated December 18, 2018. The authors are thankful to Prof. Kuppanagounder P. Elango, Department of Chemistry, Gandhigram Rural Institute (Deemed to be University), Gandhigram, India, for DNA binding studies. We are grateful to Dr. Susmita De and Mr. Mohammed Sadik N.K., Department of Applied Chemistry, CUSAT, Kerala, India, for theoretical studies. The authors are thankful to the Sophisticated Analytical Instrumentation Facility, Cochin University of Science and Technology, Kochi, India, for elemental analyses, NMR spectra and single-crystal X-ray diffraction measurements.

#### AUTHOR CONTRIBUTIONS

**Nimya Mathews:** Conceptualization; data curation; formal analysis; funding acquisition; investigation; methodology; project administration; resources; software; validation; visualization. **M. R. Prathapachandra Kurup:** Conceptualization; data curation; formal analysis; investigation; methodology; project administration; resources; software; supervision; validation; visualization.

#### CONFLICT OF INTEREST

There are no conflicts of interest.

#### SUPPLEMENTARY DATA

The following is the supporting information to this article:

Crystallographic data for the structural analysis have been deposited with the Cambridge Crystallographic Data Center as CCDC 1911171 and 1920141 for Complexes **1** and **2**, respectively. Copies of this information may be obtained free of charge via [www.ccdc.cam.ac.uk/conts/retrieving.html](http://www.ccdc.cam.ac.uk/conts/retrieving.html) or from the Director, CCDC, 12 Union Road, Cambridge, CB2, 1EZ, UK (fax: +44-1223-336-033; email: [deposit@ccdc.cam.ac.uk](mailto:deposit@ccdc.cam.ac.uk)).

#### DATA AVAILABILITY STATEMENT

The data that support the findings of this study are available in the supplementary material of this article.

#### ORCID

M.R. Prathapachandra Kurup  <https://orcid.org/0000-0002-9434-890X>

#### REFERENCES

- [1] B. Rosenberg, L. Vancamp, T. Krigas, *Nature* **1965**, *205*, 698.
- [2] L. A. Saryan, K. Mailer, C. Krishnamurti, W. Antholine, D. H. Petering, *Biochem. Pharmacol.* **1981**, *30*, 1595.
- [3] T. S. Lobana, R. Sharma, G. Bawa, S. Khanna, *Coord. Chem. Rev.* **2009**, *253*, 977.
- [4] M. Wang, L. F. Wang, Y. Z. Li, *Transition Met. Chem.* **2001**, *26*, 307.
- [5] (a) A. P. Vieira, C. A. Wegermann, A. M. D. C. Ferreira, *New J. Chem.* **2018**, *42*, 13169. (b) K. Ghosh, P. Kumar, N. Tyagi, U. P. Singh, N. Goel, A. Chakraborty, P. Roy, M. C. Baratto, *Polyhedron* **2011**, *30*, 2667. (c) Y. - P. Zhang, Z. - Y. Ma, C. - Y. Gao, X. Qiao, J.-L. Tian, W. Gu, X. Liu, J. - Y. Xu, J. - Z. Zhao, S. - P. Yan, *New J. Chem.* **2016**, *40*, 7513.
- [6] G. Barone, A. Terenzi, A. Lauria, A. M. Almerico, J. M. Leal, N. Busto, B. García, *Coord. Chem. Rev.* **2013**, *257*, 2848.
- [7] S. Delaney, M. Pascaly, P. K. Bhattacharya, K. Han, J. K. Barton, *Inorg. Chem.* **2002**, *41*, 1966.
- [8] A. Hussain, M. F. AlAjmi, M. T. Rehman, S. Amir, F. M. Husain, A. Alsalmeh, M. A. Siddiqui, A. A. AlKhedhairi, R. A. Khan, *Sci. Rep.* **2019**, *9*, 5237.
- [9] E. Pahontu, V. Fala, A. Gulea, D. Poirier, V. Tapcov, T. Rosu, *Molecules* **2013**, *18*, 8812.
- [10] N. A. Mathews, P. M. S. Begum, M. R. P. Kurup, *Appl. Organomet. Chem.* **2019**, *34*, 5294.
- [11] SMART and SAINT, Area Detector Software Package and SAX Area Detector Integration Program, Bruker Analytical X-ray; Madison, WI, USA, **1997**.
- [12] SADABS, Area Detector Absorption Correction Program; Bruker Analytical X-ray; Madison, WI, **1997**.
- [13] G. M. Sheldrick, *Acta Crystallogr.* **2015**, *C71*, 3.
- [14] L. J. Farrugia, *J. Appl. Cryst.* **2012**, *45*, 849.
- [15] K. Brandenburg, *Diamond Version 3.2g*, Crystal Impact GbR, Bonn, Germany **2010**.
- [16] (a) M. J. Frisch, G. W. Trucks, H. B. Schlegel, G. E. Scuseria, M. A. Robb, J. R. Cheeseman, J. A. Montgomery Jr., T.

- Vreven, K. N. Kudin, J. C. Burant, J. M. Millam, *GAUSSIAN 03, Revision C. 02*, Gaussian, Inc., Wallingford CT **2004**. (b) E. M. Abdalla, L. H. A. Rahman, A. A. Abdelhamid, M. R. Shehata, A. A. Alothman, A. Nafady, *Appl. Organomet. Chem.* **2020**, 5912.
- [17] A. T. Alphonsa, C. Loganathan, S. A. A. Anand, S. Kabilan, *J. Mol. Struct.* **2017**, 1130, 1018.
- [18] A. Kosiha, K. M. Lo, C. Parthiban, K. P. Elango, *Mater. Sci. Eng. C* **2019**, 94, 778.
- [19] B. Tang, F. Shen, D. Wan, B.-H. Guo, Y.-J. Wang, Q.-Y. Yia, Y.-J. Liu, *RSC Adv.* **2017**, 7, 34945.
- [20] W. J. Geary, *Coord. Chem. Rev.* **1971**, 7, 81.
- [21] E. B. Seena, M. R. P. Kurup, E. Suresh, *J. Chem. Crystallogr.* **2008**, 38, 93.
- [22] M. Vaidyanathan, R. Balamurugan, U. Sivagnanam, M. Palaniandavar, *J. Chem. Soc. Dalton Trans.* **2001**, 3498.
- [23] (a) L. Latheef, M. R. P. Kurup, *Spectrochim Acta Part a* **2008**, 70, 86. (b) N. A. Mathews, J. M. Jacob, P. M. Sabura Begum, M. R. P. Kurup, *J. Mol. Struct.* **2020**, 1202, 127319.
- [24] (a) A. Sreekanth, H.-K. Fun, M. R. P. Kurup, *Inorg. Chim. Commun.* **2014**, 7, 1250. (b) K. N. Annesrahman, G. Rohini, N. S. P. Bhuvanesh, S. Sundararaj, M. Musthafa, A. Sreekanth, *ChemistrySelect* **2018**, 3, 8118.
- [25] M. Mohanty, A. Banerjee, S. Biswal, A. Horn Jr., G. Schenk, K. Brzezinski, E. Sinn, H. Reuter, R. Dinda, *J. Inorg. Biochem.* **2020**, 203, 110908.
- [26] K. Jayakumar, M. Sithambaresan, A. A. Aravindakshan, M. R. P. Kurup, *Polyhedron* **2014**, 75, 50.
- [27] E. A. El Samanody, *Appl. Organomet. Chem.* **2018**, 32, 4586.
- [28] M. K. Shanmugaiah, K. M. Palsamy, R. Lokesh, G. N. Indra, L. Mitu, R. Jegathalaprathaban, R. Gurusamy, *Appl. Organomet. Chem.* **2018**, 33, 4762.
- [29] E. B. Seena, M. R. P. Kurup, *Spectrochim. Acta Part a* **2008**, 69, 726.
- [30] R. Rohs, I. Bloch, H. Sklenar, Z. Shakked, *Nucleic Acids Res.* **2005**, 33, 7048.
- [31] M. P. Kesavan, G. G. Vinoth Kumar, K. Anitha, L. Ravi, J. Dhavethu Raja, G. Rajagopal, J. Rajesh, *J. Photochem. Photo-biol. B: Bio.* **2017**, 173, 499.
- [32] F. Dimiza, S. Fountoulaki, A. N. Papadopoulos, C. A. Kontogiorgis, V. Tangoulis, C. P. Raptopoulou, V. Psycharis, A. Terzis, D. P. Kessissoglou, G. Psomas, *Dalton Trans.* **2011**, 40, 8555.
- [33] (a) N. Selvakumaran, N. S. P. Bhuvanesh, R. Karvembu, *Dalton Trans.* **2014**, 43, 16395. (b) A. A. Alothman, M. D. Albaqami, *Appl. Organomet. Chem.* **2020**, 34, 5827.
- [34] (a) J. Liu, T. Zhang, T. Lu, L. Qu, H. Zhou, Q. Zhang, L. Ji, *J. Inorg. Biochem.* **2002**, 91, 269. (b) A. A. A. Aziz, A. Shawky, M. M. H. Khalil, *Appl. Organomet. Chem.* **2018**, 32, 4404. (c) K. Jeyalakshmi, Y. Arun, N. S. P. Bhuvanesh, P. T. Perumal, A. Sreekanth, R. Karvembu, *Inorg. Chem. Front.* **2015**, 2, 780.
- [35] S. Banerjee, P. Ghorai, P. Brandao, D. Ghosh, S. Bhuiya, D. Chattopadhyay, S. Das, A. Saha, *New J. Chem.* **2018**, 42, 246.
- [36] B. Abulhasanv, U. Yildiz, S. Akkoc, B. Coban, *Appl. Organomet. Chem.* **2020**, 5866.
- [37] U. Yildiz, A. S. Engül, I. Kandemir, F. Cömert, S. Akkoç, B. Coban, *Bioorg. Chem.* **2019**, 87, 70.

## SUPPORTING INFORMATION

Additional supporting information may be found online in the Supporting Information section at the end of this article.

**How to cite this article:** Mathews NA, Kurup MRP. In vitro biomolecular interaction studies and cytotoxic activities of copper(II) and zinc(II) complexes bearing ONS donor thiosemicarbazones. *Appl Organomet Chem.* 2020; e6056. <https://doi.org/10.1002/aoc.6056>